# Improved trial methods for a class of generalized Bernoulli problems

Harbrecht, Helmut and Mitrou, Giannoula



Originally published as:

Harbrecht, Helmut and Mitrou, Giannoula. (2014) *Improved trial methods for a class of generalized Bernoulli problems.* Journal of mathematical analysis and applications, Vol. 420, H. 1. S. 177-194.

# Improved trial methods for a class of generalized Bernoulli problems

Helmut Harbrecht[1,*], Giannoula Mitrou[2]

*Mathematisches Institut, Universität Basel, Rheinsprung 21, 4051 Basel, Switzerland*

**Abstract**

The aim of this article is to develop improved trial methods for the solution of a generalized exterior Bernoulli free boundary problem. At the free boundary, we prescribe the Neumann boundary condition and update the free boundary with the help of the remaining Dirichlet boundary condition. Appropriate update rules are obtained by expanding the state's Dirichlet data at the actual boundary via a Taylor expansion of first and second order. The resulting trial methods converge linearly for both cases, although the trial method based on the second order Taylor expansion is much more robust. Nevertheless, via results of shape sensitivity analysis, we are able to modify the update rules such that their convergence is improved. The feasibility of the proposed trial methods and their performance is demonstrated by numerical results.

*Keywords:* free boundary problem, trial method, higher order convergence
*2000 MSC:* 35R35, 35Q99, 65P05, 76B99

## 1. Introduction

In this article, we consider a generalized version of Bernoulli's exterior free boundary problem which involves Poisson's equation and non-constant boundary data. To mathematically describe the problem under consideration, let $T \subset \mathbb{R}^2$ be a bounded domain with free boundary $\partial T = \Gamma$. Inside the domain $T$, we assume the existence of a simply connected subdomain $S \subset T$ with fixed boundary $\partial S = \Sigma$. The resulting annular domain $T \setminus \overline{S}$ is denoted by $\Omega$; see Figure 1.1 for a sketch of the geometry.

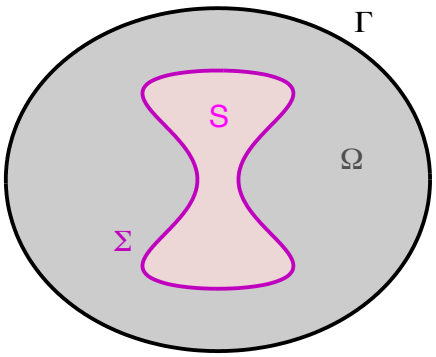


Figure 1.1: The domain $\Omega$ and its boundaries $\Gamma$ and $\Sigma$.

*Corresponding author.
*Email addresses:* helmut.harbrecht@unibas.ch (Helmut Harbrecht), giannoula.mitrou@unibas.ch (Giannoula Mitrou)
[1]This author acknowledges the support of the SNF through the project No. 200021_137668.
[2]This author acknowledges the support of the DFG priority program SPP 1253.

The generalized Bernoulli free boundary problem reads as follows: Seek the domain $\Omega$ and the state $v$ which satisfy the overdetermined boundary value problem

$$\begin{aligned} -\Delta v &= f && \text{in } \Omega \\ v &= g && \text{on } \Sigma \\ v = 0,\ \frac{\partial v}{\partial \mathbf{n}} &= h && \text{on } \Gamma. \end{aligned} \tag{1.1}$$

Here, $\mathbf{n}$ stands for the unit normal vector on $\Gamma$ and $\partial v/\partial \mathbf{n}$ denotes the normal derivative of $v$. Moreover, $f$, $g$, and $h$ are supposed to be sufficiently smooth functions which satisfy $f \geq 0$, $g > 0$ and $h < 0$ such that the solution $v$ is well defined and positive in $\Omega$.

The free boundary problem under consideration can be viewed as the prototype of a large class of stationary free boundary problems involved in many applications such as fluid dynamics, optimal design, electromagnetics and various other engineering fields. For example, the exterior magnetic shaping of liquid metals involves the exterior Poisson equation as state equation and the solution's uniqueness is ensured by a volume constraint instead by a fixed interior boundary, see e.g. [8, 21]. Also the maximization of the torsional stiffness of an elastic cylindrical bar under simultaneous constraints on its volume and bending rigidity fits in the above general setup, see [4]. We refer to [3, 5, 12] for a review of theoretical results concerning the existence and uniqueness of solutions to free boundary problems. Results on the geometric form of the boundary $\Gamma$ can be found in [1] and the references therein.

For the solution of the above free boundary problem, we choose a fixed point type method, the so-called trial method. The trial method is an iterative scheme, described by the following steps:

1. Choose an initial guess $\Gamma_0$ of the free boundary.
2. a) Solve the boundary value problem with the Neumann boundary condition on the free boundary $\Gamma_k$.
   b) Update the free boundary $\Gamma_k$ such that the Dirichlet boundary condition is approximately satisfied at the new boundary $\Gamma_{k+1}$.
3. Repeat step 2 until the process becomes stationary up to a specified accuracy.

Usually, the update is derived through a Taylor expansion and moves the boundary such that the Dirichlet boundary condition is satisfied. The use of a first order Taylor expansion has been proposed in [12, 26]. In this article, we will even use a second order Taylor expansion which, as numerical results show, is more robust. However, the trial method still convergences only linearly.

In order to obtain higher order convergence, the Neumann boundary condition at the free boundary has been substituted by a Robin boundary condition in [12, 26]. Instead, we intend to improve the convergence of the trial method without changing the boundary condition at the free boundary $\Gamma$. This is achieved by modifying the update rule appropriately.

To the several numerical schemes for the solution of free boundary problems belong parametric trial methods, as proposed in [2, 12, 25, 26], and the pseudo-solid approach, as proposed in [13, 19, 27]. The level set method for Bernoulli's problem has been used in [6, 7, 18], enjoying the property of allowing topology changes. In all these papers, however, only the Laplace equation and constant Dirichlet and Neumann data have been considered which corresponds to the original Bernoulli free boundary problem. In [23], for a related time-harmonic inverse acoustic scattering problem, an iterative method based on the idea of the analytic continuation of the field has been used. Shape optimization provides another powerful tool to solve free boundary problems, see e.g. [10, 11, 14, 16] and the references therein.

The remainder of this article is organized as follows. Section 2 is dedicated to the derivation of the trial methods based on first and second order Taylor expansions of the state's Dirichlet data at the actual boundary. In Section 3, we reformulate the boundary value problem by boundary integral equations and propose their numerical solution by the boundary element method. Some first numerical tests are presented in Subsection 3.4. They give the motivation to get involved with the convergence theory of trial methods in Section 4. It especially enables to appropriately modify the update rule such that the convergence is improved. In addition, the inexact Newton method becomes performable. The practicability of the resulting trial methods is shown by some numerical results in Section 4.5. Finally, in Section 5, the article's conclusion is drawn.

## 2. Derivation of the update rules

### *2.1. Background and motivation*

Throughout this article, we assume that the domain $T$ is starlike. We can then represent the free boundary $\Gamma$ by a parametrization $\boldsymbol{\gamma} : [0, 2\pi] \to \mathbb{R}^2$ in polar coordinates, that is

$$\Gamma := \Big\{\boldsymbol{\gamma}(s) = r(s)\mathbf{e}_r(s) : s \in [0, 2\pi]\Big\},$$

where $\mathbf{e}_r(s) = \big(\cos(s), \sin(s)\big)^T$ denotes the unit vector in the radial direction. The radial function $r(s)$ is supposed to be a positive function in $C^2_{\text{per}}([0, 2\pi])$, where

$$C^2_{\text{per}}([0, 2\pi]) = \Big\{r \in C^2([0, 2\pi]) : r^{(i)}(0) = r^{(i)}(2\pi),\ i = 0, 1, 2\Big\},$$

such that $\operatorname{dist}(\Sigma, \Gamma) > 0$.

The trial method for the solution of the free boundary problem (1.1) requires an update rule. Suppose that the actual boundary is $\Gamma_k$. Then, the corresponding state $v_k$ satisfies

$$\begin{aligned} -\Delta v_k &= f \qquad \text{in } \Omega_k \\ v_k &= g \qquad \text{on } \Sigma \\ \frac{\partial v_k}{\partial \mathbf{n}} &= h \qquad \text{on } \Gamma_k. \end{aligned} \tag{2.1}$$

The new boundary $\Gamma_{k+1}$ is now determined by moving the old boundary into the radial direction, which is expressed by the update rule

$$\boldsymbol{\gamma}_{k+1} = \boldsymbol{\gamma}_k + \delta r_k \mathbf{e}_r. \tag{2.2}$$

The update function $\delta r_k \in C^2_{\text{per}}([0, 2\pi])$ is chosen such that the desired homogeneous Dirichlet boundary condition is satisfied at the new boundary $\Gamma_{k+1}$, i.e.,

$$v_k \circ \boldsymbol{\gamma}_{k+1} \stackrel{!}{=} 0 \quad \text{on } [0, 2\pi], \tag{2.3}$$

where $v_k$ is assumed to be smoothly extended into the exterior of $\Omega_k$. The main tool to find the update function $\delta r_k$ is Taylor's expansion of the first and second order.

### *2.2. First order update rule*

The first order update rule is obtained by linearizing $v_k \circ (\boldsymbol{\gamma}_k + \delta r \mathbf{e}_r)$ with respect to the update function $\delta r$. This yields the equation

$$v_k \circ \boldsymbol{\gamma}_{k+1} \approx v_k \circ \boldsymbol{\gamma}_k + \left(\frac{\partial v_k}{\partial \mathbf{e}_r} \circ \boldsymbol{\gamma}_k\right)\delta r_k. \tag{2.4}$$

We decompose the derivative of $v_k$ in the direction $\mathbf{e}_r$ into its normal and tangential components:

$$\frac{\partial v_k}{\partial \mathbf{e}_r} = \frac{\partial v_k}{\partial \mathbf{n}}\langle \mathbf{e}_r, \mathbf{n}\rangle + \frac{\partial v_k}{\partial \mathbf{t}}\langle \mathbf{e}_r, \mathbf{t}\rangle \quad \text{on } \Gamma_k. \tag{2.5}$$

Inserting the Neumann boundary condition $\partial v_k/\partial \mathbf{n} = h$, we arrive at the first order update equation

$$F_1(\delta r_k) := v_k \circ \boldsymbol{\gamma}_k + \left[(h \circ \boldsymbol{\gamma}_k)\langle \mathbf{e}_r, \mathbf{n}\rangle + \left(\frac{\partial v_k}{\partial \mathbf{t}} \circ \boldsymbol{\gamma}_k\right)\langle \mathbf{e}_r, \mathbf{t}\rangle\right]\delta r_k \stackrel{!}{=} 0. \tag{2.6}$$

This leads to the most common update rule and has, for example, been used in [12, 18, 26]. However, there the update is performed in the normal direction rather than the radial direction which might lead to a degeneration of the domain. Notice finally that the update equation (2.6) is solvable at least in a neighbourhood of $\Gamma^\star$ since there it holds $\partial v^\star/\partial \mathbf{e}_r = h\langle \mathbf{e}_r, \mathbf{n}\rangle < 0$ due to $\partial v^\star/\partial \mathbf{t} = 0$, $h < 0$ and $\langle \mathbf{e}_r, \mathbf{n}\rangle > 0$ for starlike domains.

*2.3. Second order update rule*

The second order update rule is derived from a second order Taylor expansion of $v_k \circ (\boldsymbol{\gamma}_k + \delta r \mathbf{e}_r)$ with respect to $\delta r$, that is

$$v_k \circ \boldsymbol{\gamma}_{k+1} \approx v_k \circ \boldsymbol{\gamma}_k + \Big(\frac{\partial v_k}{\partial \mathbf{e}_r} \circ \boldsymbol{\gamma}_k\Big)\delta r_k + \frac{1}{2}\Big(\frac{\partial^2 v_k}{\partial \mathbf{e}_r^2} \circ \boldsymbol{\gamma}_k\Big)\delta r_k^2. \tag{2.7}$$

Because of our regularity assumptions on the boundary $\Gamma_k$, we are able to compute the derivatives of the twice continuously differentiable function $v_k$. Notice that, assuming more regularity of $\Gamma_k$, even a higher order Taylor expansion can be exploited here.

The directional derivative $\partial v_k/\partial \mathbf{e}_r$ included in (2.7) is computed by (2.5). Whereas, for the second order directional derivative $\partial^2 v_k/\partial \mathbf{e}_r^2$, we refer to the following lemma.

**Lemma 2.1.** *The second order derivative of $v_k$ in the direction $\mathbf{e}_r$ is given by*

$$\frac{\partial^2 v_k}{\partial \mathbf{e}_r^2} = \frac{\partial^2 v_k}{\partial \mathbf{t}^2}\{\langle \mathbf{e}_r, \mathbf{t}\rangle^2 - \langle \mathbf{e}_r, \mathbf{n}\rangle^2\} - f\langle \mathbf{e}_r, \mathbf{n}\rangle^2 + 2\Big[\frac{\partial h}{\partial \mathbf{t}} - \kappa \frac{\partial v_k}{\partial \mathbf{t}}\Big]\langle \mathbf{e}_r, \mathbf{n}\rangle\langle \mathbf{e}_r, \mathbf{t}\rangle \quad \text{on } \Gamma_k, \tag{2.8}$$

*where $\kappa = -\langle \boldsymbol{\gamma}_k'', \mathbf{n}\rangle / \|\boldsymbol{\gamma}_k'\|^2$ denotes the curvature of the boundary $\Gamma_k$.*

*Proof.* We split the second derivative of $v_k$ in the direction $\mathbf{e}_r$ into its normal and tangential components

$$\frac{\partial^2 v_k}{\partial \mathbf{e}_r^2} = \frac{\partial^2 v_k}{\partial \mathbf{n}^2}\langle \mathbf{e}_r, \mathbf{n}\rangle^2 + 2\frac{\partial^2 v_k}{\partial \mathbf{n}\partial \mathbf{t}}\langle \mathbf{e}_r, \mathbf{n}\rangle\langle \mathbf{e}_r, \mathbf{t}\rangle + \frac{\partial^2 v_k}{\partial \mathbf{t}^2}\langle \mathbf{e}_r, \mathbf{t}\rangle^2 \quad \text{on } \Gamma_k. \tag{2.9}$$

The derivative of $v_k$'s Neumann data with respect to $s$ is given by

$$\frac{\mathrm{d}}{\mathrm{d}s}\Big(\frac{\partial v_k}{\partial \mathbf{n}} \circ \boldsymbol{\gamma}_k\Big) = \|\boldsymbol{\gamma}_k'\|\Big(\frac{\partial^2 v_k}{\partial \mathbf{n}\partial \mathbf{t}} \circ \boldsymbol{\gamma}_k\Big) + \Big\langle \nabla v_k \circ \boldsymbol{\gamma}_k, \frac{\mathrm{d}\mathbf{n}}{\mathrm{d}s}\Big\rangle.$$

Due to $\mathrm{d}\mathbf{n}/\,\mathrm{d}s = \kappa\|\boldsymbol{\gamma}_k'\|\mathbf{t}$ and the Neumann boundary condition at $\Gamma_k$, this equation can be rewritten as

$$\frac{\partial^2 v_k}{\partial \mathbf{n}\partial \mathbf{t}} = \frac{\partial h}{\partial \mathbf{t}} - \kappa \frac{\partial v_k}{\partial \mathbf{t}} \quad \text{on } \Gamma_k. \tag{2.10}$$

In accordance with our smoothness assumptions, the derivatives $\partial^2 v_k/\partial \mathbf{n}^2$ and $\partial^2 v_k/\partial \mathbf{t}^2$ are coupled via the Poisson equation which implies

$$\frac{\partial^2 v_k}{\partial \mathbf{n}^2} = -\frac{\partial^2 v_k}{\partial \mathbf{t}^2} - f \quad \text{on } \Gamma_k. \tag{2.11}$$

By inserting (2.10) and (2.11) into (2.9), the latter becomes (2.8). This concludes the proof. □

Having all the terms of the second order approximation (2.7) of the left hand side of (2.3) at hand, we find the update function $\delta r_k$ from the numerical solution of the following equation:

$$F_2(\delta r_k) := F_1(\delta r_k) + \frac{1}{2}\Big\{\Big(\frac{\partial^2 v_k}{\partial \mathbf{t}^2} \circ \boldsymbol{\gamma}_k\Big)\{\langle \mathbf{e}_r, \mathbf{t}\rangle^2 - \langle \mathbf{e}_r, \mathbf{n}\rangle^2\} - (f \circ \boldsymbol{\gamma}_k)\langle \mathbf{e}_r, \mathbf{n}\rangle^2 + 2\Big[\Big(\frac{\partial h}{\partial \mathbf{t}} - \kappa\frac{\partial v_k}{\partial \mathbf{t}}\Big) \circ \boldsymbol{\gamma}_k\Big]\langle \mathbf{e}_r, \mathbf{n}\rangle\langle \mathbf{e}_r, \mathbf{t}\rangle\Big\}\delta r_k^2 \stackrel{!}{=} 0. \tag{2.12}$$

It is especially seen from this representation that the update which is computed from this second order update equation coincides with the update computed by (2.6) except for a higher order term.

*2.4. Discretization of the free boundary problem*

For the numerical computations, we discretize the radial function $r_k^n$ associated with the boundary $\Gamma_k$ by a finite Fourier series according to

$$r_k^n(s) = a_0 + \sum_{i=1}^{n-1}\{a_i \cos(is) + b_i \sin(is)\} + a_n \cos(ns). \tag{2.13}$$

This obviously ensures that $r_k^n$ is always an element of $C^2_{\mathrm{per}}([0, 2\pi])$. To determine the update function $\delta r_k^n$, represented likewise by a finite Fourier series, we insert the $m \geq 2n$ equidistantly distributed points $s_i = 2\pi i/m$ into the update equations (2.6) and (2.12), respectively:

$$F(\delta r_k^n) \stackrel{!}{=} 0 \quad \text{in all the points} \quad s_1, \ldots, s_m.$$

This is a discrete least-squares problem which can simply be solved by the normal equations in case of the first order update equation (2.6). In case of the second order update equation (2.12), the least-squares problem is nonlinear. Hence, we have to apply the Gauss-Newton method for its solution.

## 3. Solving the boundary value problem

### *3.1. Newton potential*

Since the solution $v_k$ of the state equation is required only on the boundary $\Gamma_k$ of the domain $\Omega_k$, the boundary element method is more efficient than other methods. For sake of notational convenience, we drop the index $k$ in the rest of the section. Despite Poisson's equation, the boundary element method can be applied by making the ansatz

$$v = u + N_f \tag{3.1}$$

for a suitable Newton potential $N_f$ which satisfies the equation $-\Delta N_f = f$ and a harmonic function $u$ which satisfies the boundary value problem

$$\begin{aligned} \Delta u &= 0 && \text{in } \Omega \\ u &= g - N_f && \text{on } \Sigma \\ \frac{\partial u}{\partial \mathbf{n}} &= h - \frac{\partial N_f}{\partial \mathbf{n}} && \text{on } \Gamma. \end{aligned} \tag{3.2}$$

The Newton potential has to be given analytically or computed once in advance in a sufficiently large domain $\widehat{\Omega}$ which will contain all the iterates. Since this domain can be chosen fairly simple, efficient solution techniques for the Poisson equation can easily be applied.

### *3.2. Boundary element method*

Our approach to get the system of boundary integral equations is the direct formulation based on Green's fundamental solution. In this case, the solution $u$ of (3.2) is given by Green's representation formula

$$u(\mathbf{x}) = \int_{\Gamma \cup \Sigma} \left\{ G(\mathbf{x}, \mathbf{y}) \frac{\partial u}{\partial \mathbf{n}}(\mathbf{y}) - \frac{\partial G(\mathbf{x}, \mathbf{y})}{\partial \mathbf{n}_\mathbf{y}} u(\mathbf{y}) \right\} \mathrm{d}\sigma_\mathbf{y}, \quad \mathbf{x} \in \Omega. \tag{3.3}$$

Using the jump properties of the layer potentials, we obtain the direct boundary integral formulation of the problem

$$u(\mathbf{x}) = \int_{\Gamma \cup \Sigma} G(\mathbf{x}, \mathbf{y}) \frac{\partial u}{\partial \mathbf{n}}(\mathbf{y}) \, \mathrm{d}\sigma_\mathbf{y} + \frac{1}{2} u(\mathbf{x}) - \int_{\Gamma \cup \Sigma} \frac{\partial G(\mathbf{x}, \mathbf{y})}{\partial \mathbf{n}_\mathbf{y}} u(\mathbf{y}) \, \mathrm{d}\sigma_\mathbf{y}, \quad \mathbf{x} \in \Gamma \cup \Sigma. \tag{3.4}$$

Writing the boundaries as $A, B \in \{\Gamma, \Sigma\}$, then (3.4) includes the single layer operator

$$\mathcal{V} : C(A) \to C(B), \quad (\mathcal{V}_{AB}\rho)(\mathbf{x}) = -\frac{1}{2\pi} \int_A \log \|\mathbf{x} - \mathbf{y}\| \, \rho(\mathbf{y}) \, \mathrm{d}\sigma_\mathbf{y} \tag{3.5}$$

and the double layer operator

$$\mathcal{K} : C(A) \to C(B), \quad (\mathcal{K}_{AB}\rho)(\mathbf{x}) = \frac{1}{2\pi} \int_A \frac{\langle \mathbf{x} - \mathbf{y}, \mathbf{n}_\mathbf{y} \rangle}{\|\mathbf{x} - \mathbf{y}\|^2} \rho(\mathbf{y}) \, \mathrm{d}\sigma_\mathbf{y} \tag{3.6}$$

with the densities $\rho$ being the Cauchy data of $u$ on $A$. The equation (3.4) in combination with (3.5) and (3.6) indicates the Neumann-to-Dirichlet map, which for problem (3.2) induces the following system of integral equations

$$\begin{bmatrix} \frac{1}{2}I + \mathcal{K}_{\Gamma\Gamma} & -\mathcal{V}_{\Sigma\Gamma} \\ \mathcal{K}_{\Gamma\Sigma} & -\mathcal{V}_{\Sigma\Sigma} \end{bmatrix} \begin{bmatrix} u|_\Gamma \\ \frac{\partial u}{\partial \mathbf{n}}\big|_\Sigma \end{bmatrix} = \begin{bmatrix} \mathcal{V}_{\Gamma\Gamma} & -\mathcal{K}_{\Sigma\Gamma} \\ \mathcal{V}_{\Gamma\Sigma} & -\Big(\frac{1}{2}I + \mathcal{K}_{\Sigma\Sigma}\Big) \end{bmatrix} \begin{bmatrix} \Big(h - \frac{\partial N_f}{\partial \mathbf{n}}\Big)\Big|_\Gamma \\ (g - N_f)|_\Sigma \end{bmatrix}. \tag{3.7}$$

The boundary integral operator on the left hand side of this coupled system of boundary integral equation is continuous and satisfies a Gårding inequality with respect to $L^2(\Gamma) \times H^{-1/2}(\Sigma)$ provided that $\operatorname{diam}(\Omega) < 1$. Since its injectivity follows from potential theory, this system of integral equations is uniquely solvable according to the Riesz-Schauder theory.

The next step to the solution of the boundary value problem is the numerical approximation of the integral operators included in (3.7) which first requires the parametrization of the integral equations. To that end, we insert the parametrization of the boundaries as it was described in the beginning of Section 2.1. For the approximation of the unknown Cauchy data, we use the collocation method based on trigonometric polynomials. Applying the trapezoidal rule for the numerical quadrature and the regularization technique along the lines of [17] to deal with the singular integrals, we arrive at an exponentially convergent boundary element method provided that the data and the boundaries and thus the solution are arbitrarily smooth.

### *3.3. Numerical realization of the update rules*

We briefly present the equations we solve to determine the update functions in case of Poisson's equation. The tangential derivative of $u$ is computed from the identity

$$\frac{\partial u}{\partial \mathbf{t}} \circ \boldsymbol{\gamma} = \Big\langle \nabla u \circ \boldsymbol{\gamma}, \frac{\boldsymbol{\gamma}'}{\|\boldsymbol{\gamma}'\|} \Big\rangle = \frac{1}{\|\boldsymbol{\gamma}'\|} \frac{\mathrm{d}(u \circ \boldsymbol{\gamma})}{\mathrm{d}s}.$$

In view of (3.1), the first order update results thus from the solution of

$$F_1(\delta r) = (u + N_f) \circ \boldsymbol{\gamma} + \Big[ (h \circ \boldsymbol{\gamma}) \langle \mathbf{e}_r, \mathbf{n} \rangle + \Big( \frac{1}{\|\boldsymbol{\gamma}'\|} \frac{\mathrm{d}(u \circ \boldsymbol{\gamma})}{\mathrm{d}s} + \frac{\partial N_f}{\partial \mathbf{t}} \circ \boldsymbol{\gamma} \Big) \langle \mathbf{e}_r, \mathbf{t} \rangle \Big] \delta r = 0,$$

cf. (2.6). Likewise, to compute the second order tangential derivative of $u$, we use

$$\frac{\mathrm{d}^2(u \circ \boldsymbol{\gamma})}{\mathrm{d}s^2} = \|\boldsymbol{\gamma}'\|^2 \Big( \frac{\partial^2 u}{\partial \mathbf{t}^2} \circ \boldsymbol{\gamma} \Big) + \langle \boldsymbol{\gamma}'', \mathbf{t} \rangle \Big( \frac{\partial u}{\partial \mathbf{t}} \circ \boldsymbol{\gamma} \Big) + \langle \boldsymbol{\gamma}'', \mathbf{n} \rangle \Big( \frac{\partial u}{\partial \mathbf{n}} \circ \boldsymbol{\gamma} \Big).$$

This yields the relation

$$\frac{\partial^2 u}{\partial \mathbf{t}^2} \circ \boldsymbol{\gamma} = \frac{1}{\|\boldsymbol{\gamma}'\|^2} \frac{\mathrm{d}^2(u \circ \boldsymbol{\gamma})}{\mathrm{d}s^2} - \frac{\langle \boldsymbol{\gamma}'', \mathbf{t} \rangle}{\|\boldsymbol{\gamma}'\|^3} \frac{\mathrm{d}(u \circ \boldsymbol{\gamma})}{\mathrm{d}s} + \kappa \Big( h \circ \boldsymbol{\gamma} - \frac{\partial N_f}{\partial \mathbf{n}} \circ \boldsymbol{\gamma} \Big), \tag{3.8}$$

where we substituted the Neumann data of $u$ according to the desired boundary condition at $\Gamma$, cf. (3.2). The combination of (2.12), (3.1), and (3.8) finally yields

$$\begin{aligned} F_2(\delta r) = F_1(\delta r) + \frac{1}{2} \Big\{ \Big[ \frac{1}{\|\boldsymbol{\gamma}'\|^2} \frac{\mathrm{d}^2(u \circ \boldsymbol{\gamma})}{\mathrm{d}s^2} - \frac{\langle \boldsymbol{\gamma}'', \mathbf{t} \rangle}{\|\boldsymbol{\gamma}'\|^3} \frac{\mathrm{d}(u \circ \boldsymbol{\gamma})}{\mathrm{d}s} + \kappa \Big( h \circ \boldsymbol{\gamma} - \frac{\partial N_f}{\partial \mathbf{n}} \circ \boldsymbol{\gamma} \Big) + \frac{\partial^2 N_f}{\partial \mathbf{t}^2} \circ \boldsymbol{\gamma} \Big] \{ \langle \mathbf{e}_r, \mathbf{t} \rangle^2 - \langle \mathbf{e}_r, \mathbf{n} \rangle^2 \} \\ - (f \circ \boldsymbol{\gamma}) \langle \mathbf{e}_r, \mathbf{n} \rangle^2 + 2 \Big[ \frac{\partial h}{\partial \mathbf{t}} \circ \boldsymbol{\gamma} - \frac{\kappa}{\|\boldsymbol{\gamma}'\|} \frac{\mathrm{d}(u \circ \boldsymbol{\gamma})}{\mathrm{d}s} - \kappa \Big( \frac{\partial N_f}{\partial \mathbf{t}} \circ \boldsymbol{\gamma} \Big) \Big] \langle \mathbf{e}_r, \mathbf{n} \rangle \langle \mathbf{e}_r, \mathbf{t} \rangle \Big\} \delta r^2. \end{aligned}$$

The quantities $\mathrm{d}(u \circ \boldsymbol{\gamma})/\,\mathrm{d}s$ and $\mathrm{d}^2(u \circ \boldsymbol{\gamma})/\,\mathrm{d}s^2$ which show up in the above expressions are computed by differentiating the trigonometric representation of the approximation to $u \circ \boldsymbol{\gamma}$.

*3.4. Numerical results*

In this section, we perform numerical tests in order to compare the trial methods based on the first and the second order update rule. We choose the fixed boundary $\Sigma$ kite-shaped, parameterized via

$$\boldsymbol{\gamma}_\Sigma(s) = \begin{bmatrix} -0.1\cos(s) + 0.065\cos(2s) \\ 0.15\sin(s) \end{bmatrix}.$$

As initial guess $\Gamma_0$ to the free boundary $\Gamma$, a slightly perturbed ellipse is used:

$$\boldsymbol{\gamma}_{\Gamma_0}(s) = \sqrt{0.04\cos^2(2s) + 0.06\sin^2(2s)} \begin{bmatrix} \cos(s) \\ \sin(s) \end{bmatrix}.$$

We intend to solve the free boundary problem with respect to the data

$$f(x,y) = 60, \quad g(x,y) = x^2 + y^2 + 1, \quad \text{and} \quad h(x,y) = -\lambda(x^2 + y^2 + 1),$$

where $\lambda$ is a positive constant. An appropriate Newton potential can be analytically determined, namely $N_f(x,y) = -15(x^2+y^2)$. Figure 3.1 shows the boundary $\Sigma$ and the optimal boundary $\Gamma^\star$ of the free boundary problem for different values of the parameter $\lambda$.

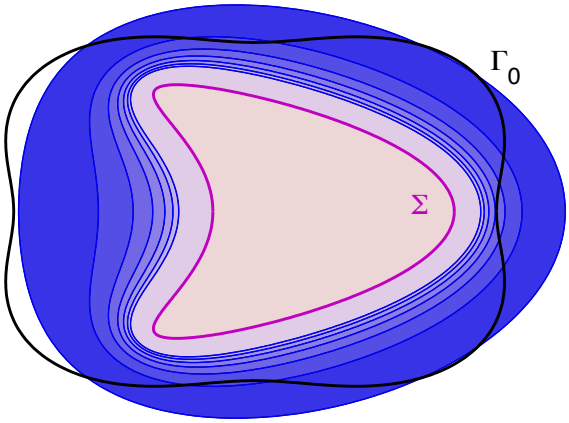


Figure 3.1: Solutions of the generalized Bernoulli free boundary problem in case of a kite-shaped interior boundary.

In Table 3.1, we present the number of boundary updates which the trial methods require in order to reach the optimal free boundary $\Gamma^\star$. The numerical setting was as follows. We used 80 degrees of freedom to represent the unknown boundary $\Gamma_k$ (i.e., $n = 40$) and 600 boundary elements per boundary. The trial method was stopped if the update function satisfied $\|\delta r\| < 10^{-8}$. The outermost boundary corresponds to $\lambda = 10$ and the innermost boundary to $\lambda = 40$. As one figures out of the table, the trial method based on the first order update converges only if the parameter $\lambda$ is small enough (row entitled "1st order update"). Whereas, the trial method based on the second order update converges for all choices of the parameter $\lambda$ (row entitled "2nd order update"). One can therefore notice that high values of $\lambda$ are more computationaly demanding.

The following modification helps to enforce convergence in case of the first order update also for large values of $\lambda$. Namely, we introduce an appropriate damping parameter $\alpha > 0$ in the update of the radial function: $r_{k+1} = r_k + \alpha\delta r$. Then, as it is seen in Table 3.1, convergence for all values of $\lambda$ is achieved for the particular choices $\alpha = 0.5$ and $\alpha = 0.8$ (rows entitled "1st order update with damping"). Nevertheless, we emphasize that there is no systematic rule of choosing the damping parameter; see Remark 4.3.

It turns out that both, the trial method based on the first order update and the trial method based on the second order update, converge linearly (see Figure 3.2). However, the trial method based on the second order update is much more robust unless we use a suitable damping for the trial method based on the first order update. The last annotation we are going to make is that, for the trial method based on the second order update, we are able to compute with more degrees of freedom for the representation of $r_k$ than for the trial method based on the first order update.

| parameter $\lambda$ | 10 | 15 | 20 | 25 | 30 | 35 | 40 |
|---|---|---|---|---|---|---|---|
| 1st order update | 14 | 20 | 23 | 31 | – | – | – |
| 1st order update with damping ($\alpha = 0.8$) | 18 | 22 | 23 | 22 | 21 | 20 | 19 |
| 1st order update with damping ($\alpha = 0.5$) | 38 | 41 | 42 | 41 | 39 | 37 | 36 |
| 2nd order update | 14 | 21 | 27 | 28 | 29 | 29 | 31 |

Table 3.1: Number of iterations of the trial method.

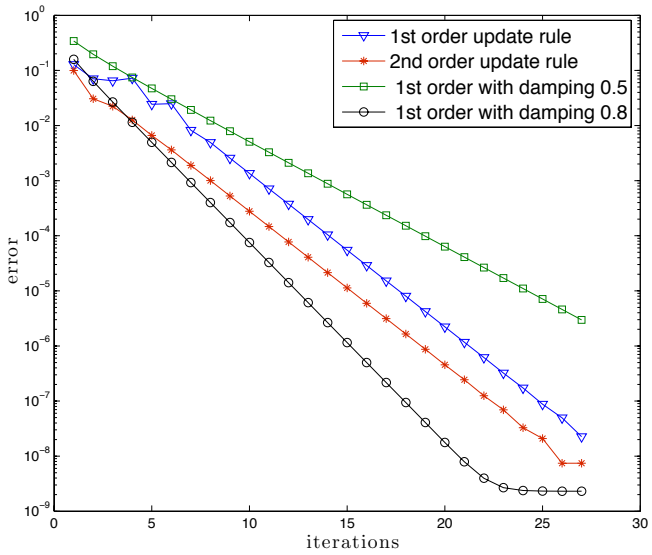


Figure 3.2: Convergence history of the trial method based on the first and second order update equation in case of $\lambda = 25$.

## 4. Convergence analysis

### *4.1. Shape sensitivity analysis*

We shall investigate the convergence of the trial method. Following the lines of [26], we explore under which conditions we gain convergence and which is the attained rate of the convergence. To that end, some results from shape sensitivity analysis are required.

Given a sufficiently smooth domain perturbation field $\mathbf{V} : \Omega \to \mathbb{R}^2$ such that $\mathbf{V}|_\Sigma = \mathbf{0}$, we can define the perturbed domain $\Omega_\varepsilon[\mathbf{V}]$ by

$$\Omega_\varepsilon := \Big\{(\mathbf{I} + \varepsilon\mathbf{V})(\mathbf{x}) : \mathbf{x} \in \Omega\Big\}.$$

Let $v$ and $v_\varepsilon$ denote the solution of (2.1) with respect to the domains $\Omega$ and $\Omega_\varepsilon$. Then, the local shape derivative $\delta v = \delta v[\mathbf{V}]$ of $v$ at $\Omega$ in the direction $\mathbf{V}$ is *formally* (see [20, 24] for a rigorous derivation) obtained by the pointwise limit

$$\delta v(\mathbf{x}) = \lim_{\varepsilon \to 0} \frac{v_\varepsilon(\mathbf{x}) - v(\mathbf{x})}{\varepsilon}, \quad \mathbf{x} \in \Omega \cap \Omega_\varepsilon.$$

The local shape derivative measures the sensitivity of the solution to (2.1) when changing the domain $\Omega$ in the direction $\mathbf{V}$. According to [9, 24], the local shape derivative can be characterized by a boundary value problem.

**Lemma 4.1.** *Given a sufficiently smooth domain perturbation field* $\mathbf{V} : \Omega \to \mathbb{R}^2$ *such that* $\mathbf{V}|_\Sigma = \mathbf{0}$*. Then, the local*

*shape derivative* $\delta v = \delta v[\mathbf{V}]$ *of the boundary value problem* (2.1) *is given as the solution of the problem*

$$\begin{aligned} \Delta \delta v &= 0 && \text{in } \Omega \\ \delta v &= 0 && \text{on } \Sigma \\ \frac{\partial \delta v}{\partial \mathbf{n}} &= \operatorname{div}_\Gamma \left( \langle \mathbf{V}, \mathbf{n} \rangle \nabla_\Gamma v \right) + \left[ \kappa h + \frac{\partial h}{\partial \mathbf{n}} + f \right] \langle \mathbf{V}, \mathbf{n} \rangle && \text{on } \Gamma. \end{aligned} \tag{4.1}$$

For more details concerning shape sensitivity analysis, we address the reader to [9, 20, 22, 24].

### *4.2. Banach's fixed point theorem*

The procedure of proving higher order convergence is based on Banach's fixed point theorem. The update rule (2.2) defines a self-mapping

$$\Phi : X \to X, \quad r \mapsto \Phi(r) = r + \delta r(r)$$

in a Banach space $X$. For the present theory, the space $X = C^2_{\text{per}}([0, 2\pi])$ will be appropriate. By construction, the update $\delta r$ vanishes at the sought free boundary $\Gamma^\star = \{\mathbf{x} \in \mathbb{R}^2 : \mathbf{x} = r^\star \mathbf{e}_r\}$. Hence, the radial function $r^\star$ which describes the boundary $\Gamma^\star$ is obviously a fixed point $r^\star = \Phi(r^\star)$ of the mapping $\Phi$. In particular, the trial method corresponds to the fixed point iteration

$$r_{k+1} = r_k + \delta r(r_k), \quad k = 0, 1, 2, \ldots.$$

According to Banach's fixed point theorem, there exists a unique solution of this fixed point iteration if the mapping $\Phi$ is contractive. The convergence rate

$$\lim_{k\to\infty} \frac{\|r_{k+1} - r^\star\|_X}{\|r_k - r^\star\|_X} = \lim_{k\to\infty} \frac{\|\Phi(r_k) - \Phi(r^\star)\|_X}{\|r_k - r^\star\|_X} = \lim_{k\to\infty} \frac{\|\delta\Phi[r_k - r^\star](r^\star)\|_X}{\|r_k - r^\star\|_X}$$

can be estimated by

$$\lim_{k\to\infty} \frac{\|r_{k+1} - r^\star\|_X}{\|r_k - r^\star\|_X} \leq \sup_{\|q\|_X = 1} \lim_{\varepsilon \to 0} \frac{\|\Phi(r^\star + \varepsilon q) - \Phi(r^\star)\|_X}{\varepsilon} = \sup_{\|q\|_X = 1} \|\delta\Phi[q](r^\star)\|_X. \tag{4.2}$$

As firstly stated in [26], we can thus deduce a sufficient condition for the convergence of the trial method. Namely, if $\sup_{\|q\|_X=1} \|\delta\Phi[q](r^\star)\|_X < 1$, then the trial method converges. If it holds in addition $\inf_{\|q\|_X=1} \|\delta\Phi[q](r^\star)\|_X > 0$, then the convergence rate is linear.

**Theorem 4.2.** *Consider the trial method based on the first order update equation* (2.6)*. Then, for a given perturbation* $q \in X$*, it holds*

$$\delta\Phi[q](r^\star) = -\frac{\delta v^\star[q] \circ \boldsymbol{\gamma}^\star}{(h \circ \boldsymbol{\gamma}^\star)\langle \mathbf{e}_r, \mathbf{n} \rangle}, \tag{4.3}$$

*where* $\boldsymbol{\gamma}^\star = r^\star \mathbf{e}_r$ *and* $\delta v^\star[q]$ *denotes the local shape derivative of* $v^\star$ *at the optimal boundary* $\Gamma^\star$ *into the direction* $\mathbf{V} \circ \boldsymbol{\gamma}^\star = q\mathbf{e}_r$.[3]

*Proof.* Define $\boldsymbol{\gamma}^\star_\varepsilon = (r^\star + \varepsilon q)\mathbf{e}_r$ and let $v^\star$ and $v^\star_\varepsilon$ denote the solutions to the underlying boundary value problems (2.1) relative to the domains $\Omega^\star$ and $\Omega^\star_\varepsilon$, i.e.,

$$\begin{aligned} -\Delta v^\star &= f && \text{in } \Omega^\star, & \qquad -\Delta v^\star_\varepsilon &= f && \text{in } \Omega^\star_\varepsilon \\ v^\star &= g && \text{on } \Sigma, & \qquad v^\star_\varepsilon &= g && \text{on } \Sigma \\ \frac{\partial v^\star}{\partial \mathbf{n}} &= h && \text{on } \Gamma^\star, & \qquad \frac{\partial v^\star_\varepsilon}{\partial \mathbf{n}} &= h && \text{on } \Gamma^\star_\varepsilon. \end{aligned}$$

[3] The local shape derivative depends only on the boundary perturbation $\mathbf{V} \circ \boldsymbol{\gamma}^\star$, see e.g. [9, 24]. Hence, we do not need to specify a particular extension of $q\mathbf{e}_r$ into the domain $\Omega^\star$.

Then, in view of the first order update equation (2.6), it holds

$$\delta r(r^\star) = -\frac{v^\star \circ \boldsymbol{\gamma}^\star}{\frac{\partial v^\star}{\partial \mathbf{e}_r} \circ \boldsymbol{\gamma}^\star} = 0 \quad \text{and} \quad \delta r(r^\star + \varepsilon q) = -\frac{v_\varepsilon^\star \circ \boldsymbol{\gamma}_\varepsilon^\star}{\frac{\partial v_\varepsilon^\star}{\partial \mathbf{e}_r} \circ \boldsymbol{\gamma}_\varepsilon^\star}.$$

Hence, we obtain

$$\begin{aligned}
\delta\Phi[q](r^\star) &= \lim_{\varepsilon\to 0} \frac{\Phi(r^\star + \varepsilon q) - \Phi(r^\star)}{\varepsilon} \\
&= \lim_{\varepsilon\to 0} \frac{r^\star + \varepsilon q + \delta r(r^\star + \varepsilon q) - r^\star - \delta r(r^\star)}{\varepsilon} \\
&= q - \lim_{\varepsilon\to 0} \frac{1}{\varepsilon} \frac{v_\varepsilon^\star \circ \boldsymbol{\gamma}_\varepsilon^\star}{\frac{\partial v_\varepsilon^\star}{\partial \mathbf{e}_r} \circ \boldsymbol{\gamma}_\varepsilon^\star}.
\end{aligned}$$

On the optimal boundary $\Gamma^\star$, the following identities are valid:

$$v^\star \circ \boldsymbol{\gamma}^\star = 0 \quad \text{and} \quad \frac{\partial v^\star}{\partial \mathbf{n}} \circ \boldsymbol{\gamma}^\star = h \circ \boldsymbol{\gamma}^\star.$$

So, assuming that $v_\varepsilon^\star$ is smoothly extended into the exterior of $\Omega_\varepsilon^\star$, we conclude

$$\frac{v_\varepsilon^\star \circ \boldsymbol{\gamma}_\varepsilon^\star}{\varepsilon} = \frac{v_\varepsilon^\star \circ \boldsymbol{\gamma}_\varepsilon^\star - v_\varepsilon^\star \circ \boldsymbol{\gamma}^\star}{\varepsilon} + \frac{(v_\varepsilon^\star - v^\star) \circ \boldsymbol{\gamma}^\star}{\varepsilon} \xrightarrow{\varepsilon\to 0} q\left(\frac{\partial v^\star}{\partial \mathbf{e}_r} \circ \boldsymbol{\gamma}^\star\right) + \delta v^\star[q] \circ \boldsymbol{\gamma}^\star$$

and

$$\frac{\partial v_\varepsilon^\star}{\partial \mathbf{e}_r} \circ \boldsymbol{\gamma}_\varepsilon^\star \xrightarrow{\varepsilon\to 0} \frac{\partial v^\star}{\partial \mathbf{e}_r} \circ \boldsymbol{\gamma}^\star = (h \circ \boldsymbol{\gamma}^\star)\langle \mathbf{e}_r, \mathbf{n}\rangle. \tag{4.4}$$

Consequently, the derivative of the mapping $\Phi$ with respect to $q$ can be simplified according to

$$\delta\Phi[q](r^\star) = q - \frac{q(h \circ \boldsymbol{\gamma}^\star)\langle \mathbf{e}_r, \mathbf{n}\rangle}{(h \circ \boldsymbol{\gamma}^\star)\langle \mathbf{e}_r, \mathbf{n}\rangle} - \frac{\delta v^\star[q] \circ \boldsymbol{\gamma}^\star}{(h \circ \boldsymbol{\gamma}^\star)\langle \mathbf{e}_r, \mathbf{n}\rangle} = -\frac{\delta v^\star[q] \circ \boldsymbol{\gamma}^\star}{(h \circ \boldsymbol{\gamma}^\star)\langle \mathbf{e}_r, \mathbf{n}\rangle}.$$

□

From this result, it is obvious that the question whether the trial method based on the first order update equation is (locally) converging or not, i.e., whether the number $\sup_{\|q\|_X=1} \|(\delta v^\star[q] \circ \boldsymbol{\gamma}^\star)/((h \circ \boldsymbol{\gamma}^\star)\langle \mathbf{e}_r, \mathbf{n}\rangle)\|_X$ is smaller than 1 or not, can be answered by inspecting the local shape derivative (4.1) at $\Gamma^\star$. It satisfies the Neumann boundary condition

$$\frac{\partial \delta v^\star}{\partial \mathbf{n}} = \left[\kappa h + \frac{\partial h}{\partial \mathbf{n}} + f\right]\langle \mathbf{V}, \mathbf{n}\rangle \quad \text{on } \Gamma^\star$$

due to $v^\star = 0$ and thus $\nabla_\Gamma v^\star = 0$ on $\Gamma^\star$. Since it in general holds

$$\left[\kappa h + \frac{\partial h}{\partial \mathbf{n}} + f\right] \neq 0 \quad \text{almost everywhere on } \Gamma^\star,$$

the local shape derivative $\delta v^\star[q]$ is nonzero for all directions $0 \neq q \in X$. Therefore, we can only expect linear convergence of the trial method[4], as already observed in the numerical experiments of Subsection 3.4.

**Remark 4.3.** In case of a damping, the self-mapping $\Phi$ is modified according to

$$\Phi : X \to X, \quad r \mapsto \Phi(r) = r + \alpha \delta r(r).$$

[4]Since $\delta v^\star[q]$ satisfies the Laplace equation with homogenous boundary condition on $\Sigma$, the Dirichlet data $\delta v^\star[q] \circ \boldsymbol{\gamma}^\star$ can only vanish if it holds $\delta v^\star[q] = 0$ in $\Omega^\star$.

Therefore, the derivative becomes

$$\delta\Phi[q](r^\star) = (1-\alpha)q - \alpha\frac{\delta v^\star[q]\circ\boldsymbol{\gamma}^\star}{(h\circ\boldsymbol{\gamma}^\star)\langle\mathbf{e}_r,\mathbf{n}\rangle}.$$

From this expression, it is not obvious how to choose the damping parameter $\alpha$ to ensure that $\sup_{\|q\|_X=1}\|\delta\Phi[q](r^\star)\|_X < 1$.

The update $\delta r_2 = \delta r_2(r)$ computed from the second order update equation (2.12) coincides with the update $\delta r_1 = \delta r_1(r)$ computed from the first order update equation (2.6) except for a higher order term, i.e., $\delta r_2(r) = \delta r_1(r) + \varepsilon(r)$ with $\|\varepsilon(r)\|_X = O(\|\delta r_1(r)\|_X^2)$. Hence, all the results about the convergence remain essentially valid also in the case of the trial method based on the second order update equation (2.12).

*4.3. Speeding up the convergence*

As we have seen before, the computation of the shape derivative $\delta v^\star[q]$ enables the evaluation of the convergence rate of the method. Hence, a question of great importance arises. What happens if $\|(\delta v^\star[q]\circ\boldsymbol{\gamma}^\star)/((h\circ\boldsymbol{\gamma}^\star)\langle\mathbf{e}_r,\mathbf{n}\rangle)\|_X \geq 1$? Can we then enforce convergence of the trial method or is it possible to obtain even superlinear convergence? A superlinearly convergent trial method for Bernoulli's free boundary problem has been proposed in [12], called the implicit Neumann method. Results on a quadratically convergent trial method can be found in [25, 26], where the solution of a Robin boundary value problem was suggested. Unfortunately, this Robin boundary value problem is only well-posed if the free boundary is convex. In contrast, our objective is to avoid the solution of a boundary value problem other than (2.1) since this would require the change of the boundary element method.

As a consequence of the observations in the previous subsection, we shall modify the self-mapping $\Phi$ according to

$$\Phi : X \to X, \quad r \mapsto \Phi(r) = r + \alpha(r)\delta r(r). \tag{4.5}$$

Notice that $r^\star$ is still a fixed point of $\Phi$. We shall now determine the function $\alpha(r) : [0, 2\pi] \to \mathbb{R}$ such that superlinear convergence of the method is ensured. In other words, we seek a function $\alpha(r)$ such that

$$\lim_{k\to\infty}\frac{\|r_{k+1}-r^\star\|_X}{\|r_k-r^\star\|_X} = \lim_{k\to\infty}\frac{\|\Phi(r_k)-\Phi(r^\star)\|_X}{\|r_k-r^\star\|_X} = \lim_{k\to\infty}\frac{\|\delta\Phi[r_k-r^\star](r^\star)\|_X}{\|r_k-r^\star\|_X} = 0. \tag{4.6}$$

Following the same procedure as in the proof of Theorem 4.2, the derivative of the mapping $\Phi$ with respect to a given direction $q$ is computed by

$$\delta\Phi[q](r^\star) = \lim_{\varepsilon\to 0}\frac{\Phi(r^\star+\varepsilon q)-\Phi(r^\star)}{\varepsilon} = q - \lim_{\varepsilon\to 0}\frac{\alpha(r^\star+\varepsilon q)}{\varepsilon}\frac{v_\varepsilon^\star\circ\boldsymbol{\gamma}_\varepsilon^\star}{\frac{\partial v_\varepsilon^\star}{\partial\mathbf{e}_r}\circ\boldsymbol{\gamma}_\varepsilon^\star}.$$

Recall that $v_\varepsilon^\star\circ\boldsymbol{\gamma}_\varepsilon^\star \to v^\star\circ\boldsymbol{\gamma}^\star = 0$ as $\varepsilon\to 0$. Thus, similar to the proof of Theorem 4.2, we conclude

$$\frac{\alpha(r^\star+\varepsilon q)}{\varepsilon}(v_\varepsilon^\star\circ\boldsymbol{\gamma}_\varepsilon^\star) = \frac{\alpha(r^\star+\varepsilon q)-\alpha(r^\star)}{\varepsilon}(v_\varepsilon^\star\circ\boldsymbol{\gamma}_\varepsilon^\star) + \alpha(r^\star)\frac{v_\varepsilon^\star\circ\boldsymbol{\gamma}_\varepsilon^\star}{\varepsilon} \xrightarrow{\varepsilon\to 0} \alpha(r^\star)\Big[q\Big(\frac{\partial v^\star}{\partial\mathbf{e}_r}\circ\boldsymbol{\gamma}^\star\Big) + \delta v^\star[q]\circ\boldsymbol{\gamma}^\star\Big].$$

In view of (4.4), we finally arrive at

$$\delta\Phi[q](r^\star) = q - \alpha(r^\star)\Big(\frac{\delta v^\star[q]\circ\boldsymbol{\gamma}^\star}{\frac{\partial v^\star}{\partial\mathbf{e}_r}\circ\boldsymbol{\gamma}^\star} + q\Big).$$

A superlinearly convergent scheme is derived if we define the function $\alpha(r)$ such that (4.6) is satisfied for the direction $q := \lim_{k\to\infty}(r_k - r^\star)/\|r_k - r^\star\|_X$ provided that this limit exists. Nevertheless, since $r^\star$ is unknown, $q$ would not be accessible even in the case of existence. Hence, we choose just $q = 1$ which corresponds to the radial direction $\mathbf{e}_r$. This leads to

$$\alpha(r) = \frac{\frac{\partial v}{\partial\mathbf{e}_r}\circ\boldsymbol{\gamma}}{\delta v[\mathbf{e}_r]\circ\boldsymbol{\gamma} + \frac{\partial v}{\partial\mathbf{e}_r}\circ\boldsymbol{\gamma}}. \tag{4.7}$$

This expression depends on the actual state $v$ and on its local shape derivative. The local shape derivative $\delta v[\mathbf{e}_r]$ can be evaluated in complete analogy to the solution of the mixed boundary value problem (4.1) by using the Neumann-to-Dirichlet map (3.7) as it was described in Section 3. Hence, one additional solve of the Neumann-to-Dirichlet map (3.7) is necessary per iteration step.

**Remark 4.4.** The condition

$$\left[\kappa h + \frac{\partial h}{\partial \mathbf{n}} + f\right] \leq 0 \quad \text{on } \Gamma^\star \tag{4.8}$$

is very often required in connection with the convergence theory of free boundary problems, see e.g. [10, 11, 28, 29]. Since it holds also $\langle \mathbf{e}_r, \mathbf{n}\rangle > 0$ in case of a starlike domain, the prescribed Neumann data of the local shape derivative $\delta v[\mathbf{e}_r]$ are negative at $\Gamma^\star$, cf. (4.1). Hence, under the condition (4.8), there holds $\delta v[\mathbf{e}_r] < 0$ in $\Omega^\star$ and thus $\delta v[\mathbf{e}_r] < 0$ at $\Gamma^\star$. As a consequence, the denominator of $(\alpha(r^\star))(s)$ is negative for all $s \in [0, 2\pi]$. We finally conclude that $\alpha(r)$ is well defined at least in a neighbourhood of $r^\star$ if (4.8) holds.

*4.4. Inexact Newton's method*

A quadratically convergent trial method is derived in case of Newton's method. It is obtained by demanding that the update function $\delta r(r)$ becomes zero:

$$\Psi(r) = \delta r(r) \stackrel{!}{=} 0.$$

Linearizing the update function around the actual boundary $r_k$ gives

$$\Psi(r_{k+1}) \approx \Psi(r_k) + \delta\Psi[r_{k+1} - r_k](r_k) \stackrel{!}{=} 0.$$

Hence, the Newton update $q$ is determined as the solution of the linear equation

$$\delta\Psi[q](r_k) \stackrel{!}{=} -\Psi(r_k). \tag{4.9}$$

In complete analogy to the proof of Theorem 4.2, the derivative of the mapping $\Psi$ with respect to a given direction $q$ is given by

$$\delta\Psi[q](r) = \lim_{\varepsilon\to 0} \frac{\Psi(r+\varepsilon q) - \Psi(r)}{\varepsilon} = -\lim_{\varepsilon\to 0} \frac{1}{\varepsilon}\left[\frac{v_\varepsilon \circ \boldsymbol{\gamma}_\varepsilon}{\frac{\partial v_\varepsilon}{\partial \mathbf{e}_r} \circ \boldsymbol{\gamma}_\varepsilon} - \frac{v \circ \boldsymbol{\gamma}}{\frac{\partial v}{\partial \mathbf{e}_r} \circ \boldsymbol{\gamma}}\right] = -\left(q + \frac{\delta v[q] \circ \boldsymbol{\gamma}}{\frac{\partial v}{\partial \mathbf{e}_r} \circ \boldsymbol{\gamma}}\right) + E[q](r).$$

The error term $E[q](r)$ issues from neglecting the derivative of the denominator multiplied with $v \circ \boldsymbol{\gamma}$ and is of order $O(\|\delta r(r)\|_X)$ for $\|q\|_X = 1$. In particular, it holds $E[q](r^\star) = 0$. Thus, to approximately solve the nonlinear equation (4.9), we perform the fixed point iteration

$$q_{\ell+1} = \delta r(r_k) - \frac{\delta v[q_\ell] \circ \boldsymbol{\gamma}}{\frac{\partial v}{\partial \mathbf{e}_r} \circ \boldsymbol{\gamma}}, \quad \ell = 0, 1, 2, \ldots.$$

A good initial guess is given by $q_0 = \delta r(r_k)$ which would be the first iterate when starting with $q_{-1} = 0$. Nevertheless, several of these inner iterations will be performed, each of which requires one solve of the Neumann-to-Dirichlet map (3.7) to calculate the local shape derivative $\delta v[q_\ell]$. To our experience, we need about 10–20 iterations to compute the (inexact) Newton update sufficiently accurate.

**Remark 4.5.** Like for the Newton scheme, the self-mapping which underlies the proposed inexact Newton method has a vanishing first order derivative at the optimal $r^\star$. This implies that the convergence order of the iterative method is quadratic.

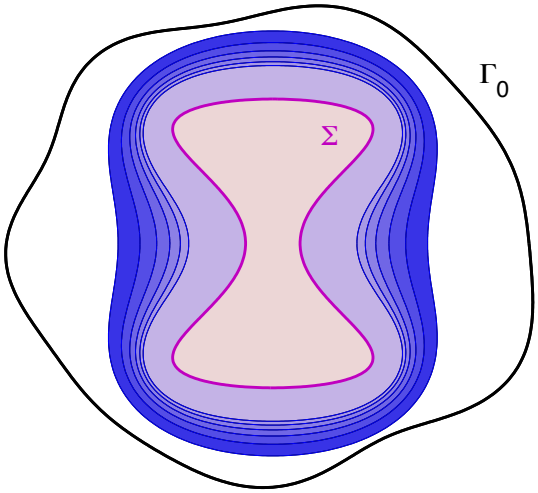


Figure 4.1: The solutions of Bernoulli's free boundary problem for different choices of the parameter $\lambda$.

*4.5. Numerical results*

In the last part of this article, we show practically the improvement in the results by two numerical examples. We consider Poisson's equation (1.1) with

$$f(x, y) = 5, \quad g(x, y) = x^2 + y^2 + 1, \quad h(x, y) = -\lambda(x^2 + y^2 + 1),$$

where $\lambda$ is a positive constant. The fixed boundary $\Sigma$ is chosen to be peanut-shaped with parametrization

$$\boldsymbol{\gamma}_\Sigma : [0, 2\pi] \to \Sigma, \quad s \mapsto \boldsymbol{\gamma}_\Sigma(s) = \begin{bmatrix} 0.03\sin(s)(1.25 + \cos(2s)) \\ 0.045\cos(s) \end{bmatrix}.$$

The solutions of the free boundary problem are depicted in Figure 4.1.

The numerical setting is as follows. We use 60 degrees of freedom to represent the unknown boundary $\Gamma_k$ (i.e., $n = 30$), 500 boundary elements per boundary, and stop the trial method if the update function satisfies $\|\delta r\| < 10^{-8}$. The random boundary seen in Figure 4.1 is the initial approximation $\Gamma_0$.

| parameter $\lambda$ | 40 | 50 | 60 | 70 | 80 | 90 |
|---|---|---|---|---|---|---|
| 1st order update | 31 | 29 | 29 | – | – | – |
| 1st order update with damping ($\alpha = 0.7$) | 14 | 17 | 20 | 22 | 23 | 23 |
| improved 1st order update | 11 | 11 | 11 | 14 | 16 | 17 |
| 2nd order update | 31 | 29 | 28 | 27 | 26 | 25 |
| improved 2nd order update | 12 | 11 | 13 | 24 | 26 | 30 |
| inexact Newton's method | 5 | 6 | 6 | 6 | 6 | 7 |

Table 4.1: Number of iteration required for convergence.

It is seen in Table 4.1 that the trial method based on the first order update equation does not always converge for the parameters $\lambda$ under consideration (row entitled "1st order update"). Whereas, the trial method based on the second order update equation converges always (row entitled "2nd order update"). Notice that a damping of the first order update by $\alpha = 0.7$ enforces convergence of the trial method based on the first order update equation (row entitled "1st order update with damping"). Nevertheless, as long as we add the update $\delta r$ with the suggested parameter $\alpha(r)$ from (4.7), then we see that the trial method is converging for both cases (rows entitled "improved 1st order update" and

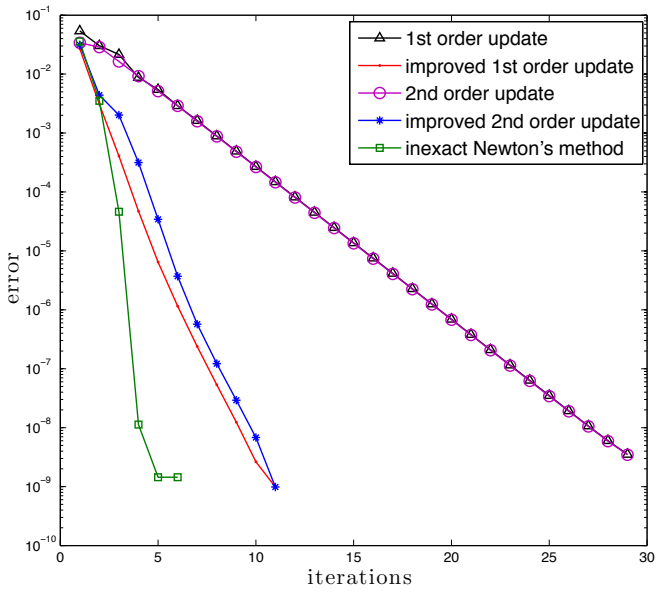


Figure 4.2: Convergence history in case of a peanut-shaped interior boundary and $\lambda \equiv 50$.

"improved 2nd order update"). Indeed, according to Figure 4.2, we obtain a nicely improved (linear) convergence rate after some burn-in where the solution is too far away from the optimal boundary $\Gamma^\star$. Finally, when we apply the inexact Newton method, we observe a further improvement of the convergence (see the row entitled "inexact Newton's method" in Table 4.1). The associated green graph in Figure 4.2 validates the quadratic convergence.

| parameter $\lambda$ | 10 | 12 | 14 | 16 | 18 | 20 |
|---|---|---|---|---|---|---|
| 1st order update | 18 | 22 | 27 | 32 | 39 | 48 |
| improved 1st order update | 14 | 18 | 21 | 28 | 35 | 38 |
| 2nd order update | 18 | 22 | 26 | 32 | 38 | 47 |
| improved 2nd order update | 12 | 16 | 22 | 28 | 26 | 44 |
| inexact Newton's method | 7 | 8 | 8 | 9 | 10 | 11 |

Table 4.2: Number of iterations of the trial methods in case of several interior boundaries.

The trial methods we have constructed are also applicable for free boundary problems with several inner boundaries. This is demonstrated by an example where the boundary $\Sigma$ is composed of the union of four circles as can be seen in Figure 4.3. We consider the original Bernoulli free boundary problem, that is

$$f(x,y) = 0, \quad g(x,y) = 1, \quad h(x,y) = -\lambda$$

in (1.1). The extension of the boundary element method introduced in Subsection 3.2 to the new topological configuration is straightforward and left to the reader. On each boundary, we apply 400 boundary elements which leads to 2000 boundary elements in all. The free boundary is discretized by 80 degrees of freedom, that is $n = 40$ in (2.13). For the initial approximation of the free boundary, we have chosen a circle. The trial method is again stopped if the update function satisfies $\|\delta r\| < 10^{-8}$.

In Table 4.2, the number of iterations of the different trial methods are listed. Now, the standard trial method converges for all chosen parameters $\lambda$ (row entitled "1st order update"). The improved 1st order update converges

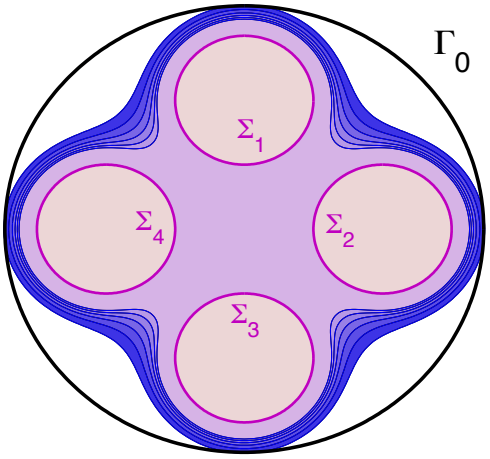


Figure 4.3: Solutions of the free boundary problem in case of several interior boundaries.

slightly faster (row entitled "improved 1st order update"). The same is observed for the related trial methods based on the second order equation (rows entitled "2nd order update" and "improved 2nd order update"). The fastest method is again the inexact Newton method (row entitled "inexact Newton's method").

## 5. Conclusions

We considered the numerical solution of generalized Bernoulli free boundary problems. On the actual domain, we approximated the solution to the boundary value problem which complies the desired Neumann boundary condition at the free boundary. This approximation is computed by a boundary element method which converges exponentially in case of smooth data. We then analyzed and applied trial methods which are based on update rules arising from first and second order Taylor series of the violated Dirichlet boundary condition at the free boundary. It turns out that an update computation based on a second order Taylor expansion of the Dirichlet data at the actual interface leads to a much more stable scheme. Moreover, by computing the local shape derivative to the boundary value problem under consideration, we were able to modify the trial method such that the convergence is improved considerably. In particular, a Newton-type method yields quadratical convergence rates.

## References

[1] A. Acker, *On the geometric form of Bernoulli configurations*, Math. Methods Appl. Sci., 10 (1988), pp. 1–14.
[2] A. Acker, *How to approximate the solutions of certain free boundary problems for the Laplace equation by using the contraction principle*, Z. Angew. Math. Phys. 32 (1981), pp. 22–33.
[3] H. W. Alt and L. A. Caffarelli, *Existence and regularity for a minimum problem with free boundary*, J. Reine Angew. Math., 325 (1981), pp. 105–144.
[4] N. V. Banichuk and B. L. Karihaloo, *Minimum-weight design of multi-purpose cylindrical bars*, Internat. J. Solids Structures, 12 (1976), pp. 267–273.
[5] A. Beurling, *On free-boundary problems for the Laplace equation*, Sem. on analytic functions, Inst. Adv. Stud. Princeton, (1957), pp. 248–263.
[6] F. Bouchon, S. Clain, and R. Touzani, *Numerical solution of the free boundary Bernoulli problem using a level set formulation*, Comput. Methods Appl. Mech. Engrg., 194 (2005), pp. 3934–3948.
[7] ———, *A perturbation method for the numerical solution of the Bernoulli problem*, J. Comput. Math., 26 (2008), pp. 23–36.
[8] O. Colaud and A. Henrot, *Numerical approximation of a free boundary problem arising in electromagnetic shaping*, SIAM J. Numer. Anal., 31 (1994), pp. 1109–1127.
[9] M. C. Delfour and J.-P. Zolésio, *Shapes and geometries*, vol. 22 of Advances in Design and Control, Society for Industrial and Applied Mathematics (SIAM), Philadelphia, PA, 2nd ed., 2011.
[10] K. Eppler and H. Harbrecht, *Efficient treatment of stationary free boundary problems*, Appl. Numer. Math., 56 (2006), pp. 1326–1339.

[11] ———, *Tracking Neumann data for stationary free boundary problems*, SIAM J. Control Optim., 48 (2009/10), pp. 2901–2916.
[12] M. Flucher and M. Rumpf, *Bernoulli's free-boundary problem, qualitative theory and numerical approximation*, J. Reine Angew. Math., 486 (1997), pp. 165–204.
[13] J. Haslinger and R.A.E. Mäkinen, *Introduction to shape optimization. Theory, approximation, and computation*, Society for Industrial and Applied Mathematics (SIAM), Philadelphia, PA, 2003.
[14] J. Haslinger, T. Kozubek, K. Kunisch, and G. Peichl, *Shape optimization and fictitious domain approach for solving free boundary problems of Bernoulli type*, Comput. Optim. Appl., 26 (2003), pp. 231–251.
[15] K. Ito, K. Kunisch and G. Peichl, *Variational approach to shape derivatives for a class of Bernoulli problems*, J. Math. Anal. Appl., 314 (2006), pp. 126–149.
[16] R. Kress, *Linear integral equations*, vol. 82 of Applied Mathematical Sciences, Springer-Verlag, New York, 2nd ed., 1999.
[17] C. M. Kuster, P. A. Gremaud, and R. Touzani, *Fast numerical methods for Bernoulli free boundary problems*, SIAM J. Sci. Comput., 29 (2007), pp. 622–634.
[18] P.A. Sackinger, P.R. Schunk, R.R. Rao, A Newton-Raphson pseudo-solid domain mapping technique for free and moving boundary problems. A finite element implementation, J. Comput. Phys., 125 (1996), pp. 83–103.
[19] F. Murat and J. Simon, *Etude de probléme d'optimal design*, in Proceedings of the 7th IFIP Conference on Optimization Techniques: Modeling and Optimization in the Service of Man, Part 2, London, UK, 1976, Springer-Verlag, pp. 54–62.
[20] M. Pierre and J.-R. Roche, *Computation of free surfaces in the electromagnetic shaping of liquid metals by optimization algorithms*, Eur. J. Mech. B/Fluids, 10 (1991), pp. 489–500.
[21] O. Pironneau, *Optimal shape design for elliptic systems*, Springer series in computational physics, Springer, New York, 1984.
[22] P. Serranho, *A hybrid method for inverse obstacle scattering problems*, PhD thesis, Georg-August-Universität Göttingen, 2007.
[23] J. Sokolowski and J.-P. Zolésio, *Introduction to shape optimization*, vol. 16 of Springer Series in Computational Mathematics, Springer-Verlag, Berlin, 1992. Shape sensitivity analysis.
[24] T. Tiihonen, *Shape optimization and trial methods for free boundary problems*, RAIRO Modél. Math. Anal. Numér., 31 (1997), pp. 805–825.
[25] T. Tiihonen and J. Järvinen, *On fixed point (trial) methods for free boundary problems*, in Free boundary problems in continuum mechanics (Novosibirsk, 1991), vol. 106 of Internat. Ser. Numer. Math., Birkhäuser, Basel, 1992, pp. 339–350.
[26] J.I. Toivanen, J. Haslinger, and R.A.E. Mäkinen, *Shape optimization of systems governed by Bernoulli free boundary problems*, Comput. Methods Appl. Mech. Engrg., 197 (2008), pp. 3803–3815.
[27] K. G. van der Zee, E. H. van Brummelen, and R. de Borst, *Goal-oriented error estimation and adaptivity for free-boundary problems: The domain-map linearization approach*, SIAM J. Sci. Comput., 32 (2010), pp. 1064–1092.
[28] K. G. van der Zee, E. H. van Brummelen, and R. de Borst, *Goal-oriented error estimation and adaptivity for free-boundary problems: The shape linearization approach*, SIAM J. Sci. Comput., 32 (2010), pp. 1093–1118.